H.E.S.S. Observations of LS 5039

Mathieu de Naurois

Astrophysics and Space Science manuscript No.
(will be inserted by the editor)

Mathieu de Naurois for the H.E.S.S. Collaboration.

H.E.S.S. Observations of LS 5039

Discovery of the 3.9 days orbital periodicity in Very High Energy γ-rays.

Received: date / Accepted: date

Abstract Recent observations of the binary system LS 5039 with the High Energy Stereoscopic System (H.E.S.S.) revealed that its Very High Energy (VHE) γ-ray emission is modulated at the 3.9 days orbital period of the system. The bulk of the emission is largely confined to half of the orbit, peaking around the inferior conjunction epoch of the compact object. The flux modulation provides the first indication of γ-ray absorption by pair production on the intense stellar photon field. This implies that the production region size must be not significantly greater than the gamma-gamma photosphere size (~ 1 AU), thus excluding the large scale collimated outflows or jets (extending out to ~ 1000 AU). A hardening of the spectrum is also observed at the same epoch between 0.2 and a few TeV which is unexpected under a pure absorption scenario and could rather arise from variation with phase in the maximum electron energy and/or the dominant VHE γ-ray production mechanism. This first-time observation of modulated γ-ray emission allows precise tests of the acceleration and emission models in binary systems.

Keywords gamma rays: observations · X-rays: binaries · individual objects: LS 5039 (HESS J126-148)

PACS 95.85.Pw · 97.80.-d

1 Introduction

In the commonly accepted paradigm, microquasars consist of a stellar mass black hole fed by a massive star. They can exhibit superluminous radio jets[22], and hints for the presence of an accretion disk. These *scaled down* versions of Active Galactic Nuclei (AGN) also show, due to their much lower mass, variability on timescales shorter by several order of magnitudes (down to minutes or even seconds) that can be used to constrain the accretion and ejection scenarios (e.g. [15]).

It has been suspected for a long time that these object could emit, through similar acceleration mechanisms as in AGN (leptonic or hadronic processes) high energy radiation up to the Very High Energy gamma-ray (VHE) domain, and that VHE radiation could give insight on the very central engine. The discovery of VHE emission from LS 5039 by HESS[2] and shortly after from LS I $+61^\circ$ 303 by MAGIC[6] confirmed this longstanding issue and established VHE astronomy as a powerful diagnostic probe of these objects.

LS 5039, identified in 1997[26] as a massive X-ray binary system with faint radio emission[19], was resolved in 2000[27] into bipolar mildly relativistic radio jets ($v \sim 0.2$ c) emanating from a central core, thus placing it into the *microquasar class*. The detection of radio and variable X-ray emission[10] and its possible association with the EGRET source 3EG J1824-1514[27] suggests the presence of multi-GeV particles possibly accelerated in jets. LS 5039 is indeed the only object simultaneously detected in X-ray and radio in the field of view of the unidentified EGRET source[31].

The binary system LS 5039 (Fig 1) consists of a massive 06.5V star in a $\sim$ 3.9 day mildly eccentric orbit ($e = 0.35$)[11] around a compact object whose exact nature (black hole or neutron star) is still under debate. Under the assumption of pseudo-synchronization, Casares and collaborators[11] constrain the compact object mass in the black hole range ($M_X = 3.7^{+1.3}_{-1} M_\odot$) and obtain a low system inclination ($i \sim 25^\circ$), but a neutron star at higher inclination ($i \sim 60^\circ$) might still remain possible[14].

M. de Naurois
Laboratoire de Physique Nucléaire et de Hautes Energies
4 place Jussieu, 75252 Paris Cedex 05
Tel.: +33-1-44272324
Fax: +33-1-44274638
E-mail: denauroi@in2p3.fr

2 H.E.S.S. Observations

The High Energy Stereoscopic System (H.E.S.S.) is an array of four identical Atmospheric Cherenkov Telescopes

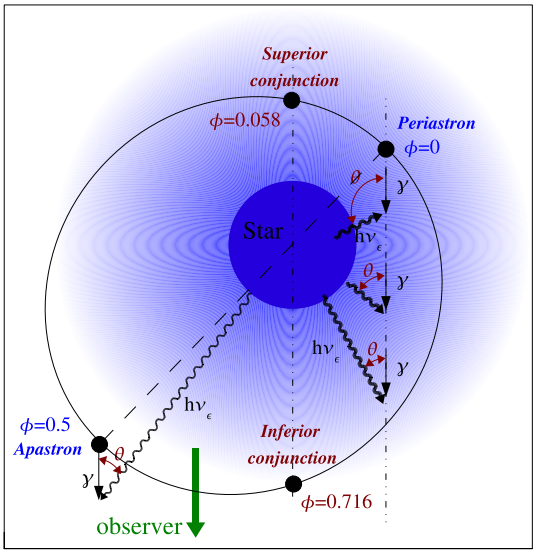

Fig. 1 Orbital geometry of the binary system LS 5039 viewed from above and using the orbital parameters derived in[11]. From [3]. Shown are: phases (ϕ) of minimum (*periastron*) and maximum (*apastron*) binary separation; epoch of superior and inferior conjunctions occurring when the compact object and the star are aligned along the observer line-of-sight.

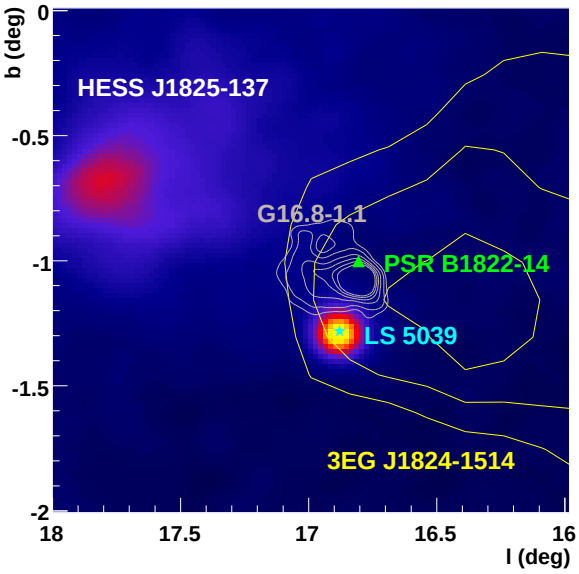

Fig. 2 H.E.S.S. excess sky map around LS 5039, smoothed by the instrument point spread function. The blue star denotes the position of the VLBA source. The yellow contours correspond to the 68%, 95% and 99% confidence level region of the EGRET source 3EG J1824-1514. The extended source HESS J1825-137 observed in the same field of view can serve as a cross-check for timing-analysis.

(ACT)[4, and references therein] located in the Southern Hemisphere (Namibia, 1800 m a.s.l.) and sensitive to γ-rays above 100 GeV.

LS 5039 was serendipitously detected in 2004 during the H.E.S.S. galactic scan[2]. The 2004 observations have been followed up by a deeper observation campaign[3] in 2005, leading to a total dataset of 69.2 hours of observation after quality selection. To optimize the coverage over the orbit, the observations were spread over more than six months, resulting in a wide range of observation conditions. The observation zenith angles are in particular distributed between $\sim 5°$ and $\sim 65°$, resulting in a trigger threshold varying between ~ 100 GeV and ~ 1 TeV.

Data were analysed using two separate calibrations[1] and analysis pipelines. The results presented here are based on the log-likelihood comparison of the shower images with a precalculated semi-analytical model[12].

3 Results

After selection cuts, a total of 1969 γ-ray events were found within $0.1°$ of the VLBA radio position of LS 5039[30], leading to a statistical significance of 40σ (Fig. 2). The best fit position is, in Galactic Coordinates, $l = 16.879°$, $b = -1.285°$ with statistical and systematic uncertainties of respectively $\pm 12''$ and $\pm 20''$. This position is compatible within 1σ with the VLBA position (denoted as a blue star in Fig. 2) and with the Chandra source. We obtain an upper limit of $28''$ (at 1σ) on the VHE source extension.

3.1 Timing Analysis

The runwise VHE γ-ray flux at energies ≥ 1 TeV was decomposed into its frequency components using the Lomb-Scargle periodogram[33] (Fig. 1) which is appropriate for unevenly sampled datasets such as those collected by H.E.S.S.

In order to reduce the effect of the varying instrument threshold, all events were used in the lightcurve determination and the runwise flux normalisation was extracted under the assumption of an average photon index derived from all data ($\Gamma = 2.23$ for $dN/dU \propto E^{-\Gamma}$. The average index assumption in this method notably increases the statistics and contributes only to a small error on the derived flux above 1 TeV).

An obvious peak in the Lomb-Scargle periodogram occurs at the period 3.9078 ± 0.0015 days, consistent with the orbital period determined by Caseres *et al.*[11] (3.90603 ± 0.00017) and excluding the earlier period of 4.4267 ± 0.0005 days determined by McSwain et al[20, 21]. The peak is highly significant, with a chance probability of $\sim 10^{-20}$ before trials (estimated via Monte-Carlo simulation of random fluxes time-series at the observations times as well as random shuffling of observed fluxes) and less than 10^{-15} after trials. Other peaks with chance probability less than 10^{-7}-10^{-8} are present in the periodogram.

Fig 3, middle panel, shows the effect of subtracting a pure sinusoid at the orbital period. The orbital peak disappears as expected, but also the numerous satellite

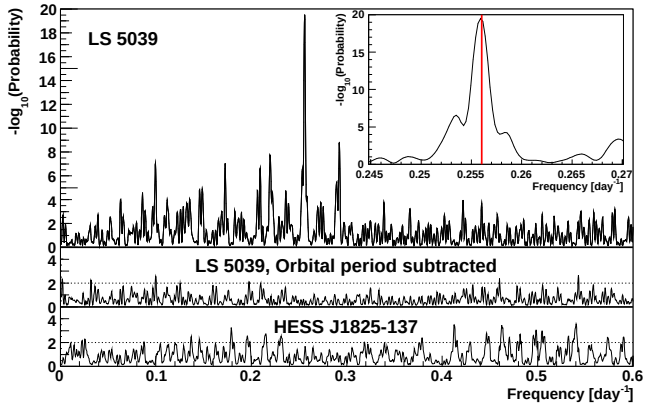

Fig. 3 Lomb-Scargle (LS) periodogram of the VHE runwise flux of LS 5039 above 1 TeV (Chance probability to obtain the LS power vs. frequency).From [3]. Zoom: inset around the highest peak, which corresponds to a period of 3.9078 ± 0.0015 days. This period is found to be compatible with the orbital period determined by Caseres *et al.*[11] and denoted as a red line on the inset. Middle: LS periodogram of the same data after subtraction of a pure sinusoidal component at the orbital period of 3.90603 days. The orbital peak is removed as expected, but also the satellite due to beat of the orbital period with various instrumental periods (see text). Bottom: LS periodogram obtained on HESS J1825-137 using the same dataset (HESS J1825-137 is observed in the same field of view.)

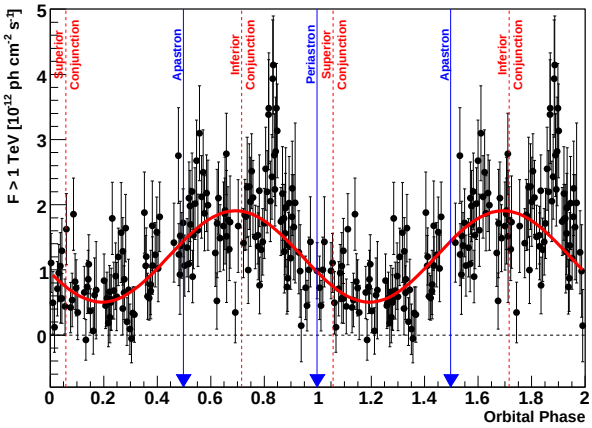

Fig. 4 Phasogram (Integral run-by-run γ-ray flux above 1 TeV as function of orbital phase) of LS 5039 from H.E.S.S. data from 2004 to 2005, using the orbital ephemeris of[11]. Each run is ~ 28 minutes. Two full phase periods are shown for clarity. The vertical blue arrows depict the respective phases of minimum (*periastron*) and maximum (*apastron*) binary separation. The vertical dashed red lines show the respective phases of inferior and superior conjunction, when the star and the compact object are aligned along the observer's line of sight. From [3].

peaks, thus confirming that these peaks are beat periods of the orbital period with the various gaps present in the H.E.S.S. dataset (day-night cycle, moon period, annual period). The bottom panel of the same figure shows the result obtained on the neighbouring source HESS J1825-137 observed in the same field of view as LS 5039. The HESS J1825-137 periodogram doesn't show any statistically significant peak, thus demonstrating that the observed periodicity is genuinely associated with LS 5039.

3.2 Flux Modulation

The runwise Phasogram (Fig 4) of integral flux at energies ≥ 1 TeV vs. orbital phase (ϕ) shows an almost sinusoidal behaviour, with the bulk of the emission largely confined in a phase interval $\phi \sim 0.45$ to 0.9, covering about half of the orbital period. The thick red line in Fig 4 represents the component at the orbital frequency determined with the Lomb-Scargle coefficients. The emission maximum ($\phi \sim 0.7$) appear to lag behind the apastron epoch and to align better with the *inferior conjunction* ($\phi = 0.716$), when the compact object lies in front of the massive star (see Fig. 1). The VHE flux minimum occurs at phase ($\phi \sim 0.2$), slightly further along the orbit than *superior conjunction* ($\phi = 0.058$).

Neither evidence for long-term secular variations in the VHE flux independent of the orbital modulation nor any other modulation period are found in the presented H.E.S.S. data.

3.3 Spectral Modulation

Due to changing environment with orbital phase (magnetic field strength, stellar photon field, relative position of compact object and star with respect to observer, ...), the VHE γ-ray emission spectrum is expected to vary along the orbit. In such a binary system, the compact object environment can be modeled with a relatively good accuracy, and the spectral modulation can therefore serve as a quite important diagnostic tool for disentangling the possible acceleration, cooling and absorption processes.

We first define two broad phase interval: **INFC** centered on the inferior conjunction ($0.45 < \phi \leq 0.9$) and its complementary **SUPC** centered on the superior conjunction, corresponding respectively to high and low flux states. Fig 5 shows the VHE spectral energy distribution for these two phase intervals. The high state is consistent with a hard power law with index $\Gamma = 1.85 \pm 0.06_{\rm stat} \pm 0.1_{\rm syst}$ with and exponential cutoff at $E_0 = 8.7 \pm 2.0$ TeV. In contrast, the spectrum for low state is compatible with a relatively steep ($\Gamma = 2.53 \pm 0.06_{\rm stat} \pm 0.1_{\rm syst}$) pure power law extending from 200 GeV to ~ 20 TeV. The spectral shapes of these two states are mutually incompatible at the level of $\sim 2 \times 10^{-6}$. Interestingly, the flux appears to be almost unmodulated at 200 GeV as well as around 20 TeV, whereas the modulation is maximum around a few (~ 5) TeV.

When going to smaller phase interval (0.1 phase bins), the statistics at high energy becomes too low to efficiently distinguish between power-law and more complicated shapes. Fig 6 shows the results (photon index and

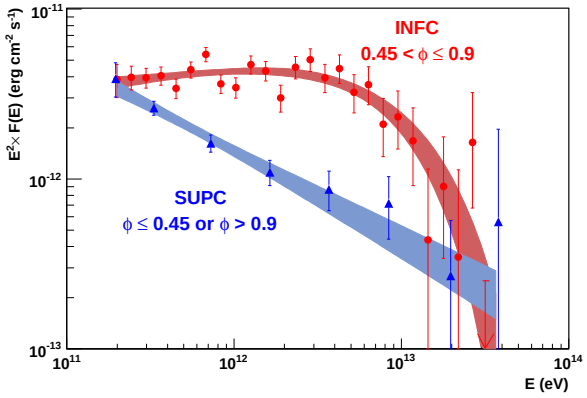

Fig. 5 Very high energy spectral energy distribution of LS 5039 for the two broad orbital phase intervals defines in the text: **INFC** $0.45 < \phi \leq 0.9$ (red circles) and its complementary **SUPC** (blue triangles). The shades regions represent the 1σ confidence bands on the fitted functions. Both spectral are mutually incompatible at the level of $\sim 2\times10^{-6}$. A clear spectral hardening is occurring in the 200 GeV to a few TeV range during the **INFC** phase interval. From [3].

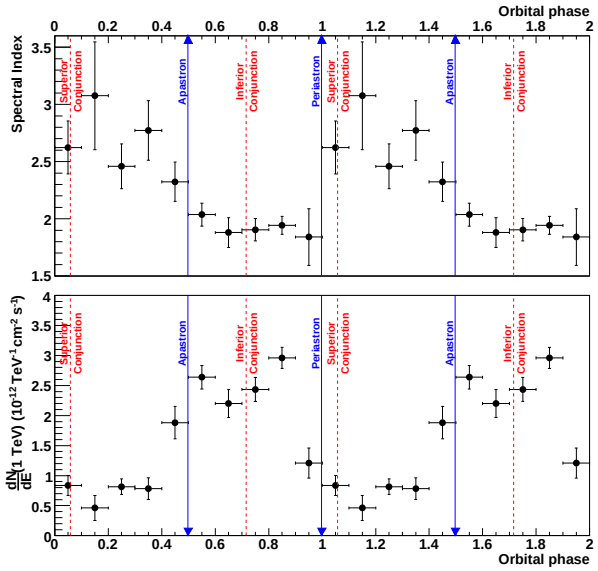

Fig. 6 Top: Fitted pure power-law photon index vs. phase interval of width $\Delta\phi = 0.1$. Bottom: Differential flux at 1 TeV for the same phase interval. From [3].

differential flux at 1 TeV) of a pure power-law fit of the high energy spectra in 0.1 orbital phase bins (restricted to energies below 5 TeV to avoid systematic effect introduced by the high state cutoff).

The flux normalisation and photon index are strongly correlated, the flux being higher when the spectrum is harder and vice-versa, as shown in Fig 7. The correlation factor is found to be $r \sim 0.8$. The photon index varies by more than one unit along the orbit, whereas the flux normalization varies by a factor of more than 5. Interestingly, a similar effect, however in a smaller variation range, was found in X-rays[10] where the photon index

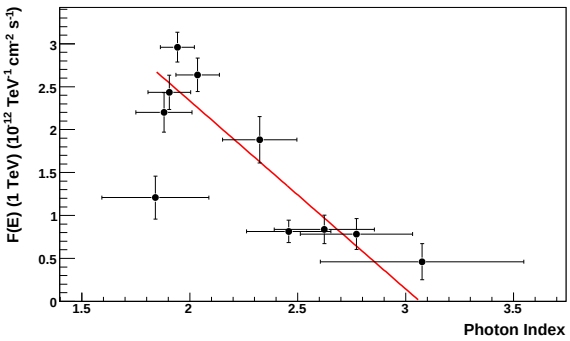

Fig. 7 Differential flux at 1 TeV vs. photon index. The red line shows the best linear fit (correlation factor $r = 0.8$).

was found to vary between 1.7 and 2.2 with time. However, the X-ray phasogram exhibited a different picture than the VHE one, with a flux maximum at $\phi \sim 0.2$ (close to the VHE flux minimum) and a second peak around $\phi \sim 0.8$ better aligned with the VHE flux.

4 Interpretation

4.1 Gamma-Ray production

The basic paradigm of VHE γ-ray production requires the presence of particles accelerated to multi-TeV energies and a target comprising photons (for γ-ray production through Inverse Compton effect) and/or matter of sufficient density (for γ-ray production through pion decay in hadronic processes, e.g. [32]). Several model classes are available to explain VHE emission from microquasars, differencing one from the other by the nature of accelerated particles and/or the location of the acceleration region. In jet-based models, particle acceleration could take place directly inside and along the jet, e.g. [9, and references therein], and also in the jet termination shock regions[16]. Non-jet scenarios are also available, e.g. [18,14], where the emission arises from the interaction of a pulsar wind with the stellar companion equatorial wind.

In LS 5039, the strong observed modulation provides new information about the physical processes in microquasars, placing in particular strong constraints on the location of the acceleration region.

4.2 Modulated absorption by pair creation

VHE γ-rays produced close enough to the stellar companion will unavoidably suffer severe absorption via pair production (e^+e^-) on its intense photon field. Due to the angular dependence of the pair creation cross-section and threshold, the optical depth will strongly depend on the alignment between the γ-ray production region, the star and the observer, leading to an orbital modulation

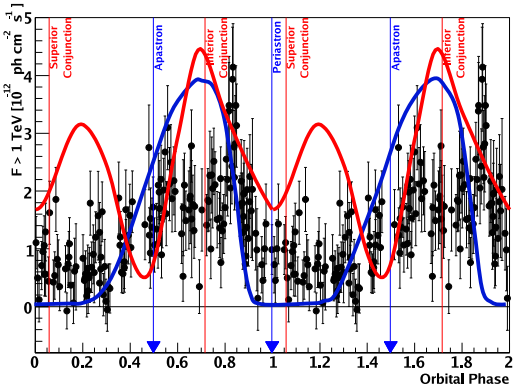

Fig. 8 Comparison of the observed phasogram (black points) with the expected flux modulation under a pure absorption scenario (blue line, adapted from [14]) and under a accretion disk-jet scenario (red line adapted from [28]). In the accretion disk-jet scenario the modulation of the accretion rate of the stellar wind along the orbit is responsible for a modulation of the jet injection and therefore for a modulation of the particle acceleration in the jet.

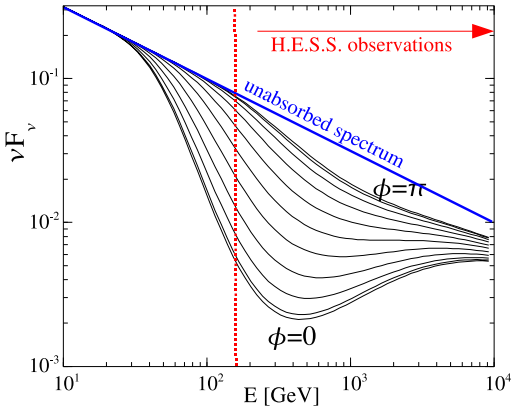

Fig. 9 Expected effect of the absorption on the γ-ray spectrum for different orbital phases. Adapted from [8]. The blue line denotes the primary unabsorbed spectrum. The black lines show the absorbed spectra for various orbital phases range between 0° and 180° (bottom to top). The sharply peaked pair production cross-section is expected to produce a dip in the observed γ-spectrum just above the pair production production threshold, in the $200 - 500$ GeV.

of the VHE γ-ray flux [29,25,8,13,7]. For the orbital geometry of LS 5039, a flux minimum is expected at the phase of inferior conjunction, where the effect of the minimum absorption threshold and the maximum column density adds up. The overall expected modulation for an emission close to the compact object (Fig. 8, blue line adapted from [14]) agrees quite well with the observed picture, suggesting that absorption plays an important role in the observed modulation.

However, its has to be noted that a signal is observed by H.E.S.S. around phase $\phi = 0$, which is unexpected under a pure absorption scenario. Detailed treatment of pair cascades, e.g. [7], in which the VHE γ-ray energy is reprocessed towards somewhat lower values, might help solving this issue. Another key expectation from the absorption scenario is that the strongest absorption, and hence modulation, should occur in the energy range $E \sim 0.2$ to 2 TeV [13,8] depending on orbital phase. Fig. 9, adapted from [8], shows the expected evolution of the VHE spectrum with phase. The flux dip at absorption maximum will produce a spectral softening at low energy ($\sim\leq 500$GeV) around phase $\phi \sim 0$, and a spectral hardening above. This picture is not consistent with the observed spectral modulation (Fig. 5) with notably an almost unmodulated flux at $\sim$ 0.2 TeV, thus suggesting that additional processes must be considered.

4.3 Modulated particle acceleration

VHE γ-ray production can be produced by accelerated electrons through the inverse-Compton (IC) scattering of stellar photons of the companion star, and/or accelerated hadrons through their interaction with surrounding photons and particles. In this scenario, the efficiency of VHE γ-ray production will peak around periastron, reflecting the higher target photon density.

The high temperature of the companion star means that IC γ-ray production proceeds primarily in the deep Klein-Nishina regime (where the IC cross-section is sharply reduced compared to the Thompson regime). Due to changing magnetic field strength and target photon density along the orbit, the maximum electron energy will be increased by a factor of roughly 10 between periastron and apastron, where the IC cooling becomes less efficient (for a more detailed discussion, see [3]). This might agree quite well with the observed spectral modulation. Moreover, synchrotron cooling takes over IC cooling above some energy $\epsilon \approx 6[(B/\mathrm{G})(d/R_*)]^{-1}$ changing with orbital phase. Much stronger synchrotron losses[24] would then produce a phase dependent spectral break, with a break energy lower by a factor of ~ 10 at periastron.

Other effects such as angular dependence of IC scattering[17] could also introduce spectral hardening at apastron phase.

4.4 Modulated particle injection

In an accretion disk-jet scenario, orbital modulation could arise from modulation of the jet injection rate. Paredes et al[28] propose a leptonic jet model for LS 5039, where a slow equatorial stellar wind induces a modulation of accretion rate (maximum shortly after periastron). An additional stream wind formed next to periastron is required to reproduce the doubled-peak X-ray lightcurve.

Their predicted VHE orbital modulation (Fig 8, red line) does not agree well with the observed orbital modulation. In particular, the enhancement in accretion rate shortly after periastron is not observed. However, complication arise from the detail treatment of absorption effect, which is this case depends on the assumption of

the position of γ-ray production along the jet. In particular, emission in the small scale jets would produce a similar absorption pattern as in Fig 8, blue line.

5 Conclusion

New observations by HESS have established orbital modulation of the VHE γ-ray flux and energy spectrum from the XRB LS 5039. The flux vs. orbital phase profile provides the first indication for γ-ray absorption within an astrophysical source, suggesting that a large part of the VHE γ-ray production region lies inside the pair absorption photosphere (within ~ 1 AU) around the massive stellar companion. However, not all of the observed effects can be explained by absorption alone. A detailed study is now required to fully explain these new observations and understand the complex relationship between γ-ray absorption and production processes within these binary systems.

Acknowledgements The support of the Namibian authorities and of the University of Namibia in facilitating the construction and operation of H.E.S.S. is gratefully acknowledged, as is the support by the German Ministry for Education and Research (BMBF), the Max Planck Society, the French Ministry for Research, the CNRS-IN2P3 and the Astroparticle Interdisciplinary Programme of the CNRS, the U.K. Particle Physics and Astronomy Research Council (PPARC), the IPNP of the Charles University, the South African Department of Science and Technology and National Research Foundation, and by the University of Namibia. We appreciate the excellent work of the technical support staff in Berlin, Durham, Hamburg, Heidelberg, Palaiseau, Paris, Saclay, and in Namibia in the construction and operation of the equipment.

References

1. Aharonian, F., et al. (HESS Collaboration): Calibration of cameras of the H.E.S.S. detector. Astropart. Phys. **22** 109-125 (2004)
2. Aharonian, F., et al. (HESS Collaboration): Discovery of very high-energy gamma-rays associated with an X-ray binary. Science **309**, 746 (2005)
3. Aharonian, F., et al. (HESS Collaboration): 3.9 day orbital modulation in the TeV gamma-ray flux and spectrum from the X-ray binary LS 5039. A&A, *submitted* (2006) and astro-ph/0607192
4. Aharonian, F., et al. (HESS Collaboration): Observations of the Crab Nebula with H.E.S.S.. A&A, *in press* (2006) and astro-ph/0607333
5. Aharonian, F., et al. (HESS Collaboration): A possible association of the new VHE gamma-ray source HESS J1825-137 with the pulsar wind nebula G18.0-0.7. A&A **442**, L25-L27 (1005)
6. Albert, J., et al.: Variable Very High Energy Gamma-Ray Emission from the Microquasar LS I +61 303, Science **312**, 1771 (2006)
7. Bednarek, W.: Propagation of very high energy gamma-rays inside massive binaries LS 5039 and LSI +61° 303. MNRAS **368**, 579-591 (2006)
8. Böttcher M., Dermer C.D.: Photon-Photon Absorption of Very High Energy Gamma Rays from Microquasars: Application to LS 5039 ApJ. **634**, L81 (2005)
9. Bosch-Ramon V., Paredes J.M.: A numerical model for the γ-ray emission of the microquasar LS 5039 Orbital X-Ray Variability of the Microquasar LS 5039. A&A **417**, 1075 (2004)
10. Bosch-Ramon V., Paredes J.M., Ribó M., et al.: Orbital X-Ray Variability of the Microquasar LS 5039. ApJ. **628**, 388 (2005)
11. Casares, J., Ribó, M., Ribas, I., Paredes, J.M., et al.: A possible black hole in the γ-ray microquasar LS 5039. MNRAS **364**, 899 (2005)
12. de Naurois M., et al.: Analysis methods for Atmospheric Cerenkov Telescopes. Proc. Towards a Network of Atmospheric Cherenkov Detectors VII (Palaiseau) p.149.
13. Dubus, G.: Gamma-ray absorption in massive X-ray binaries. A&A **451**, 9-18 (2006)
14. Dubus, G.: Gamma-ray binaries: pulsars in disguise?. A&A *submitted* (2006) and astro-ph/0605287 (2005) and astro-ph/0607247
15. Fender, R.P., et al.: Rapid infrared flares in GRS 1915+105: evidence for infrared synchrotron emission. MNRAS **290**, L65-L69 (1997)
16. Heinz S., Sunyaev R.: Cosmic rays from microquasars : A narrow component to the CR spectrum? A&A **390**, 751-766 (2002)
17. Khangulyan D., Aharonian F. AIP Conf. Proc. **745**, 359 (2005)
18. Maraschi L., Treves A.: A model for LSI 61°303. MNRAS **194**, 1 (1981)
19. Marti, J., Paredes, J. M.and Ribo, M. : The system LS 5039: a new massive radio emitting X-ray binary. A&A **338**, L71-L74 (1998)
20. McSwain, M. V., et al.: The Orbit of the Massive X-Ray Binary LS 5039. A&A **558** L43-L46 (2001)
21. McSwain, M. V., et al.: The N Enrichment and supernova ejection of the runaway microquasar LS 5039. A&A **600** 927-938 (2004)
22. Mirabel, I.F., Rodriguez L.F.: A Superluminal Source in the Galaxy. Nature **371**, 46 (1994)
23. Mirabel, I.F.: Very Energetic gamma-Rays from Microquasars and Binary Pulsars. Science **312** 1759-1760 (2006)
24. Moderski R., Sikora M., Coppi P.S., Aharonian F., Klein-Nishina effects in the spectra of non-thermal sources immersed in external radiation fields. MNRAS **363**, 954 (2005)
25. Moskalenko I.V.: TeV emission from close binarieius. Spa. Sci. Rev., 72, **593** (1995)
26. Motch, C., et al. : New massive X-ray binary candidates I from the ROSAT Galactic Plane Survey. A&A **323** 853-875 (1997)
27. Paredes, J.M., Martí J., Ribó M., Massi M.: Discovery of a High-Energy Gamma-Ray-Emitting Persistent Microquasar. Science **288**, 2340 (2000)
28. Paredes, J.M., Bosch-Ramon V., Romero G.E.: Spectral energy distribution of the gamma-ray microquasar LS 5039. A&A **451**, 259 (2006)
29. Protheroe R.J., Stanev T.: Constraints on models of Cygnus X-3 from high-energy gamma-ray absorption at source. ApJ 322, **838** (1987)
30. Ribó, M., et al: LS 5039: A runaway microquasar ejected from the galactic plane. A&A **384**, p.954-964 (2002)
31. Ribó, M.: Discovery and study of the microquasar LS 5039 and a search for new microquasars, PhD Thesis, Universtat de Barcelona (2002)
32. Romero, G.E., et al.: Hadronic gamma-ray emission from windy microquasars. A&A **410**, L1 (2003)
33. Scargle, J.D., Studies in astronomical time series analysis. II - Statistical aspects of spectral analysis of unevenly spaced data: ApJ **263**, 835 (1982)